THE JOURNAL OF PHYSICAL CHEMISTRY B

Article

Cite This: J. Phys. Chem. B 2018, 122, 12260−12270

pubs.acs.org/JPCB

Introduction of Positive Charges into Zwitterionic Phospholipid Monolayers Disrupts Water Structure Whereas Negative Charges Enhances It

Saranya Pullanchery,[†] Tinglu Yang,[†] and Paul S. Cremer*[,†,‡]

[†]Department of Chemistry and [‡]Department of Biochemistry and Molecular Biology, Penn State University, University Park, Pennsylvania 16802, United States

Supporting Information

ABSTRACT: The interfacial water structure and phosphate group hydration of 1,2-dioleoyl-*sn*-glycero-3-phosphatidylcholine monolayers were investigated at air/water interfaces. Both vibrational sum frequency spectroscopy (VSFS) and Langmuir monolayer compression measurements were made. The PC lipids oriented water molecules predominantly through their phosphate-choline (P-N) dipoles and carbonyl moieties. Upon the introduction of low concentrations of 1,2-dioleoyl-3-trimethylammonium propane (DOTAP), a positively charged double chain surfactant, the TAP headgroups were attracted to the phosphate moieties on adjacent PC lipids. This attraction caused the monolayers to contract, expelling water molecules that were hydrogen bonded to the phosphate groups. Moreover, amplitude of the OH stretch signal decreased. At higher DOTAP concentrations, the positive charge on the monolayer caused an increase in the area per headgroup and water molecules in the near-surface bulk region became increasingly aligned. Under these latter conditions, the OH stretch amplitude was linearly proportional to the surface potential. By contrast, introducing 1,2-dioleoyl-*sn*-glycero-3-phosphatidylglycerol, a negatively charged lipid, did not change the area per lipid or the phosphate−water hydrogen bonding network. As the interfacial potential grew more negative, the OH stretch amplitude increased continuously. Significantly, changes in the interfacial water spectrum were independent of the chemistry employed to create the positive or negative interfacial potential. For example, Ca^{2+} and tetracaine (both positively charged) disrupted the water structure similarly to low DOTAP concentrations, whereas SCN^- and ibuprofen (both negatively charged) enhanced the water structure. These results suggest a direct correlation amongst the interfacial water structure, area per lipid, and surface charge density.

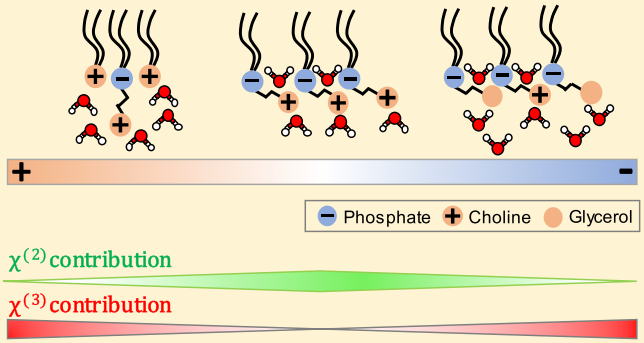

Lipids in biological membranes interact strongly with water molecules surrounding their headgroups. Such hydration water acts as a mediator for all chemical interactions at the membrane surface. Vibrational sum frequency spectroscopy (VSFS), a second-order nonlinear optical technique,[1−5] has proven to be a powerful tool for obtaining vibrational spectra of lipid/water interfaces.[6−10] VSFS studies of charged lipid and surfactant monolayers have demonstrated that water dipoles next to positively and negatively charged interfaces have opposite orientations. Specifically, the lone pairs on oxygen atoms point toward positively charged interfaces whereas they point away from negatively charged ones.[11,12] By contrast, PC, the most abundant lipid component in biological membranes, is zwitterionic and has a more complex water structure associated with it.[13−15] Namely, the structure is dominated by the P-N dipole that consists of a phosphate and a choline moiety separated by two methylene units (Figure 1A). Recent VSFS studies have demonstrated that the PC headgroup can orient water dipoles through the phosphate, choline, and the carbonyl moieties.[14,16−18] In fact, these three types of ordered water have different orientations and account for most of the intensity in the OH stretch region of the VSFS spectrum. Moreover, the interfacial OH stretch spectrum adjacent to PC lipids has been monitored in the presence of a variety of charged moieties in the subphase, including Ca^{2+},[19] SCN^-,[20] various drug molecules,[21,22] and nanoparticles.[23] On the basis of existing studies, however, it is difficult to draw definitive conclusions on the correlation between the surface charge and the interfacial water spectrum. As such, there is a need for a set of systematically controlled experiments wherein the surface charge density is varied, while holding the ionic strength and the phase behavior of the lipid membrane constant.

In pure PC membranes, the P-N dipole orients almost parallel to the membrane/water interface (Figure 1B, center).[24−26] The dipole undergoes two types of conformational changes after charged moieties are introduced.[27−33] In

Received: August 30, 2018
Revised: October 22, 2018
Published: December 13, 2018

DOI: 10.1021/acs.jpcb.8b08476
J. Phys. Chem. B 2018, 122, 12260−12270

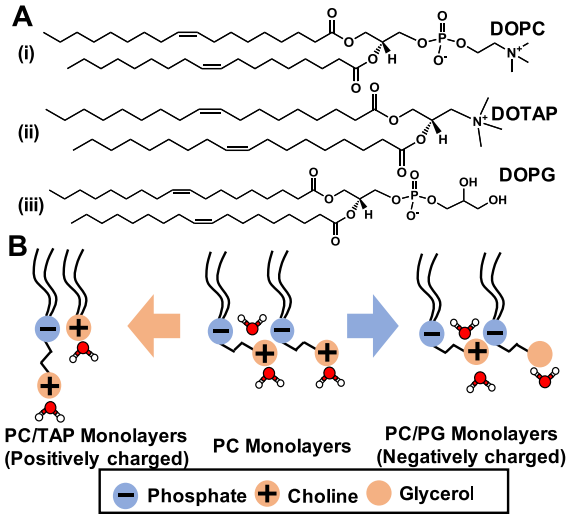

Figure 1. (A) Structures of (i) 1,2-dioleoyl-*sn*-glycero-3-phosphatidylcholine (DOPC), (ii) 1,2-dioleoyl-3-trimethylammonium propane (DOTAP), and (iii) 1,2-dioleoyl-*sn*-glycero-3-phosphatidylglycerol (DOPG). (B) A schematic diagram illustrating the effects of low concentrations of positively and negatively charged lipids on the interfacial water structure next to the P-N dipole of PC headgroups.

the presence of positively charged species, the N^+ end of the dipole moves substantially toward the water phase (Figure 1B, left), but moves very slightly toward the membrane interior when negatively charged moieties are added (Figure 1B, right). This remarkable generality in the response of the lipid P-N dipole to charged species leads to the question as to how the interfacial water spectrum responds as charges are introduced. For strictly neutral interfaces, the intensity in the sum frequency spectrum (I_{VSFS}) is proportional to the square of the second-order nonlinear susceptibility ($\chi^{(2)}$) of the interfacial water molecules and can be expressed as follows[34]

$$I_{VSFS} \propto |\chi^{(2)} E_{VIS} E_{IR}|^2 \quad (1)$$

where E_{VIS} and E_{IR} are the electric fields generated by the visible and IR beams, respectively. For charged interfaces, however, water molecules in the bulk are also ordered by the surface potential. These molecules have been shown to contribute to the nonlinear optical signal through the third-order nonlinear susceptibility ($\chi^{(3)}$), as described by eq 2[35−39]

$$I_{VSFS} \propto |\chi^{(2)} E_{VIS} E_{IR} + \chi^{(3)} E_{VIS} E_{IR} \Phi(0)|^2 \quad (2)$$

where $\Phi(0)$ is the potential at the interface.

The $\chi^{(3)}$ construct has been utilized to understand the changes in the nonlinear optical signal as a function of surface potential. Rao et al. measured the second harmonic generation (SHG) signal in solutions with 1-palmitoyl-2-oleoyl-*sn*-glycero-3-phosphocholine (POPC) vesicles, which were initially uncharged.[40] Significantly, the SHG signal decreased as positively charged cell penetrating TAT peptides were introduced. From these experiments, the authors concluded that the $\chi^{(3)}$ contribution had the opposite sign from $\chi^{(2)}$, resulting in a net decrease in the SHG signal. It should be noted, however, that the addition of the positively charged species may also alter the contribution from directly bound water molecules, thus altering the $\chi^{(2)}$ contribution. Tian and co-workers demonstrated that the VSFS spectrum from water at a fatty acid/water interface can be separated into $\chi^{(2)}$ and $\chi^{(3)}$ terms.[41] They found that the $\chi^{(2)}$ contribution from the hydrogen bonded layer of interfacial water varied significantly as a function of surface potential, at least at lower pH values. The importance of accounting for changes in the $\chi^{(2)}$ term as the surface potential increased was also recently pointed out by Gibbs and co-workers for silica/water interfaces.[42] These authors demonstrated that deprotonated silanols can align water at high pH through hydrogen bonding and noted that such changes should be treated through the $\chi^{(2)}$ term. Of course, accounting for changes in $\chi^{(2)}$ should be crucial for understanding water signals from PC membranes as charged species can substantially alter lipid−lipid interactions as well as the area per lipid.

Herein, we have investigated the changes in the interfacial OH stretch spectrum of DOPC monolayers while introducing varying concentrations of positively charged DOTAP and negatively charged DOPG lipids into the monolayer (structures provided in Figure 1A). Unlike ions, small molecules, or peptides, charged lipids can be directly embedded into the monolayer, even at very high mole fractions of the charged component. Using these systems, we found that changes in the amplitude of the water peaks tracked linearly with changes in surface potential at sufficiently high mol % DOTAP. This fact could be exploited to deconvolve the 3200, 3450, and 3640 cm^{-1} peaks into separate $\chi^{(2)}$ and $\chi^{(3)}$ contributions. For all three peaks, at low concentrations of the positively charged moiety, the changes in the water signal were dominated by the change in the $\chi^{(2)}$ response as the area per lipid contracted. Significantly, the 3450 and 3640 cm^{-1} peaks were found to be better reporters of the $\chi^{(2)}$ response than the one at 3200 cm^{-1}. Changes in these higher frequency peaks were also more closely correlated to the area per lipid than the 3200 cm^{-1} peak. For all three peaks, the changes in $\chi^{(3)}$ became the dominant contribution to changes in amplitude at higher mol % DOTAP. By contrast to these results, the area per lipid was not significantly changed as DOPG was added. As a result of the unchanged area per lipid, the $\chi^{(2)}$ contribution was not significantly affected, and changes in all three water peaks could be explained predominantly from the $\chi^{(3)}$ contribution even for relatively low DOPG concentrations.

To better understand the origins of the trends seen in the OH stretch region, we also measured the phosphate vibrational spectrum of DOPC in the presence of DOTAP and DOPG. This allowed us to probe the hydrogen bonding network around the phosphate moiety in the presence of positively and negatively charged species. It was found that the degree of phosphate hydration as judged by the peak position of the phosphate stretch resonance was correlated with the OH stretch amplitude from H_2O. This result indicated that the phosphate−water hydrogen bonding network was a key factor influencing the VSFS water spectrum next to DOPC, via a $\chi^{(2)}$ contribution to the signal. Specifically, DOTAP lipids dehydrated the phosphate moiety and resulted in a decrease in the OH stretch amplitude and therefore an attenuated $\chi^{(2)}$ contribution. By contrast, negatively charged DOPG lipids enhanced the hydration. Finally, changes in the VSFS spectra of DOPC lipids in the presence of Ca^{2+}, SCN^-, tetracaine, and ibuprofen were monitored to test the generality of the findings obtained with charged lipids. The results were quite similar to the direct embedding of charged lipids. Namely, positively charged species decreased the water structure, whereas negatively charged species enhanced it.

DOI: 10.1021/acs.jpcb.8b08476
J. Phys. Chem. B 2018, 122, 12260−12270

RESULTS AND DISCUSSION

Water Structure Next to DOPC Monolayers in the Presence of Positively and Negatively Charged Lipids. Mixed Langmuir monolayers of DOPC were formed at the air/water interface with varying concentrations of DOTAP and DOPG lipids. VSFS spectra with 0, 10, and 100 mol % DOTAP are shown in Figure 2A, whereas spectra with 0, 10, and 100 mol % DOPG are provided in Figure 2B. Spectra at additional concentrations of DOTAP and DOPG, along with their fits, are provided in Figure S1. The three broad peaks in the OH stretch region from DOPC were assigned to water molecules hydrogen bonded to the phosphate group (3200 cm^{-1}), water molecules ordered by the choline moiety (3450 cm^{-1}), and water molecules in the vicinity of the carbonyl groups close to the hydrophobic tail portion of the lipids (3640 cm^{-1}).[14,16,18] The signs associated with these oscillators were positive, negative, and positive. The signs for all vibrational stretches were confirmed by using the maximum entropy method (MEM) calculations from the intensity spectra (Figure S2).[43,44]

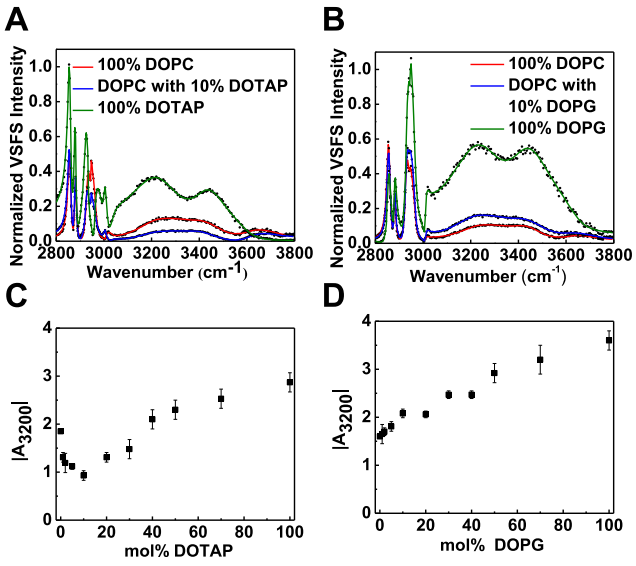

Figure 2. Effects of positively and negatively charged lipids on the interfacial OH stretch spectra of DOPC. (A) VSFS spectra of Langmuir monolayers of DOPC (red), 10 mol % DOTAP mixed with DOPC (blue), and 100% DOTAP (green). (B) VSFS spectra of Langmuir monolayers of DOPC (red), 10 mol % DOPG mixed with DOPC (blue), and 100% DOPG (green). The spectra were measured at a surface pressure of 17 mN/m on a buffer subphase containing 10 mM Tris and 100 mM NaCl at pH 7.4. The black dots are experimental data points and the solid lines are fits to the spectra (details on spectral acquisition and fitting are provided in the SI). Absolute values of the fitted 3200 cm^{-1} amplitudes (A_{3200}) of DOPC with (C) DOTAP and (D) DOPG, as a function of the charged lipid concentration. Error bars represent standard deviations from 3 to 4 measurements.

As can be seen by comparing Figure 2A,B, changes in the OH stretch region induced by DOTAP and DOPG differed substantially. The intensity of the OH stretch peaks in the VSFS spectrum decreased upon the addition of 10 mol % DOTAP to the monolayer (blue curve in Figure 2A) relative to pure DOPC. As greater concentrations of DOTAP were introduced, the water spectral features then increased (green curve in Figure 2A). By contrast, increasing the concentration of DOPG in the DOPC monolayer yielded a continuous increase in the OH stretch peak (Figure 2B). The absolute values of the fitted amplitudes from the 3200 cm^{-1} peak (Tables S1 and S2) are plotted in Figure 2C,D as a function of the DOTAP and DOPG concentrations in the monolayer, respectively. As can be seen, a continuous increase in the absolute value of the 3200 cm^{-1} amplitude above 10 mol % DOTAP and DOPG was observed. This should be expected, as the build-up of surface charge generated an interfacial electric field, which oriented more water molecules, leading to increased sum frequency signal. The low concentration dip with DOTAP, however, suggested that a different mechanism was at work in this concentration regime.

Molecular Mechanism for the Changes in Water Structure of DOPC upon Introduction of DOTAP and DOPG. The changes in VSFS intensity in the OH stretch region should be the result of a reorientation of interfacial water molecules, a change in their number density, or a combination of both.[37,45,46] As the overall surface charge flips from positive to negative or vice-versa, water molecules are expected to undergo reorientation. This should result in a sign change for the amplitude. Indeed, this has been previously observed at the alumina/water interface,[47] titania/water interface,[48] and silica/water interface.[42] In the case of DOPC, water dipoles contributing to the 3200 cm^{-1} peak flipped their average net orientation between 10 and 20 mol % DOTAP (Figure S2, Table S1). With the addition of DOPG, the sign of the amplitude for the 3200 cm^{-1} peak remained positive and continued to increase in intensity (Figure S2, Table S2). The former results confirmed the role of reorientation as a first significant factor in the attenuation of the water peaks when low concentrations of positive charge were introduced.

The second factor contributing to the dip with added DOTAP should be a change in the number density of OH oscillators. This will occur because replacement of the PC headgroup by a TAP headgroup should disrupt the phosphate hydration network, whereas this would not occur when replacement with a PG headgroup is made. In fact, a simple model can be formulated to explain the decrease in number density of oriented interfacial water molecules upon the addition of positively charged lipids as opposed to negatively charged ones. As noted in the introduction, the P-N dipoles of DOPC headgroups are known to lie almost parallel to the interface in the absence of charged lipids (Figure 1B, center).[26] In this arrangement, the water molecules contributing to the 3200 cm^{-1} peak form a hydrogen bonding network by bridging adjacent phosphate moieties. At low DOTAP concentrations, the positively charged trimethylammonium moiety is electrostatically attracted to the phosphate groups on adjacent DOPC lipids (Figure 1B, left). This results in a reduced headgroup area for DOPC and reorients the P-N dipole toward the surface normal.[32,33] Such a reduction in area should, in turn, displace water molecules that were initially hydrogen bonded between adjacent phosphates. The loss of water molecules would therefore result in an attenuation of the 3200 cm^{-1} peak. By contrast, DOPG has a phosphate moiety in its headgroup, similar to DOPC. As a result, addition of DOPG to DOPC monolayers should leave the average headgroup area and the phosphate−water hydrogen bonding network unperturbed (Figure 1B, right). Moreover, the headgroup of DOPG has a glycerol moiety, which can directly hydrogen bond with water

DOI: 10.1021/acs.jpcb.8b08476
J. Phys. Chem. B 2018, 122, 12260−12270

molecules, yielding an overall increase in the number of water molecules hydrating the headgroup.

According to the model in Figure 1B, two clear changes are expected to occur in the monolayer. First, the area per lipid should contract as positively charged DOTAP molecules are introduced, but not when negatively charged DOPG molecules are added. Second, the phosphate group should dehydrate in the presence of DOTAP, but retain its hydration in the presence of DOPG. These predictions can each be directly tested. Specifically, the changes in the area per lipid can be measured using surface pressure−area isotherms, whereas the dehydration of the phosphate group can be probed by measuring the VSFS spectrum of the phosphate stretch in the presence of positively and negatively charged lipids. The phosphate symmetric stretch is expected to blue shift as positive charges are introduced, but no such blue shift should occur as negative charges are added.[49,50]

Surface pressure−area isotherms of DOPC monolayers with increasing concentrations of DOTAP and DOPG were measured to experimentally verify changes in the average area per lipid. The values that were obtained at 17 mN/m are plotted in Figure 3A as a function of mol % DOTAP. As can be seen, the average area per lipid followed a trend that was similar to the absolute value of the 3200 cm^{-1} amplitude (Figure 2C). Specifically, the area per lipid decreased at low mol % DOTAP, followed by an increase at higher concentrations. The decrease in area at low mol % is consistent with attractive headgroup interactions and a reorientation of the P-N dipole toward the surface normal, as discussed above (Figure 1B, left). At sufficiently high mol % DOTAP, the electrostatic repulsion between DOTAP headgroups became dominant, and a reversal of this trend was observed. By contrast, the average area per lipid did not change substantially with increasing mol % DOPG, within the error bars of our measurements (Figure 3B). This is the case despite the introduction of the negatively charged moiety. Indeed, the phosphate−water hydrogen bonding network is probably the key factor in constraining the average area per lipid headgroup in mixed PC/PG lipid membranes.

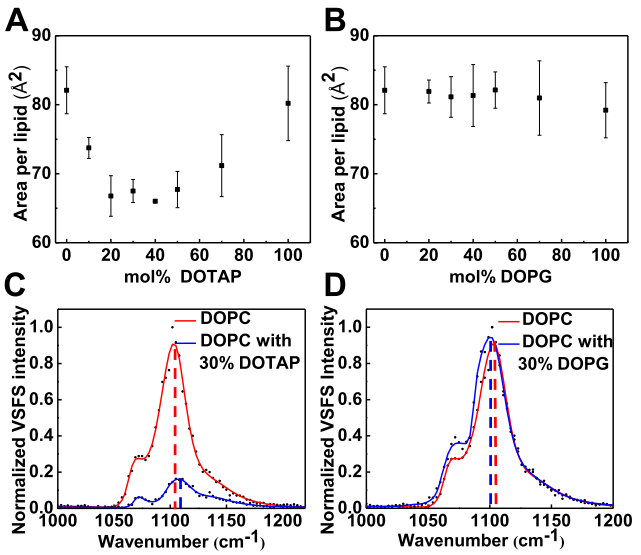

Figure 3. Average area per lipid of mixed monolayers of (A) DOPC/DOTAP and (B) DOPC/DOPG measured at a surface pressure of 17 mN/m. The error bars correspond to the standard deviation from three to four measurements. Complete sets of surface pressure−area isotherms are provided in Figure S3. (C) VSFS spectra of the phosphate stretch from pure DOPC (red) and in the presence of 30 mol % DOTAP (blue). (D) VSFS spectra of the phosphate stretch from pure DOPC (red) and in the presence of 30 mol % DOPG (blue). All spectra were measured at a surface pressure of 17 mN/m on a buffer subphase containing 10 mM Tris and 100 mM NaCl at pH 7.4. MEM analysis of these spectra is provided in Figure S4.

Since the average area per lipid reached a minimum between 20 and 50 mol % DOTAP, the phosphate groups should be relatively dehydrated in this concentration range. The PO_2^- symmetric stretch peak is highly sensitive to the local hydrogen bonding environment.[49−51] When the phosphate moiety hydrogen bonds to adjacent water molecules, electron density from the O−P−O− moiety is donated to the antibonding (σ^*) orbital of the O−H bond on water.[52] This weakens and elongates the O−P−O− bonds, resulting in a red shift of the PO_2^- symmetric stretch. The vibrational frequency of the PO_2^- symmetric stretch can therefore be used to probe the dehydration or enhanced hydration of the phosphate moiety. Figure 3C,D shows the effects of DOTAP and DOPG on the vibrational frequency of the PO_2^- symmetric stretch. The phosphate stretch region in the VSFS spectrum of DOPC (same spectrum shown in red in each panel) has several peaks originating from the phosphate and ester stretches. The prominent peak around 1105 cm^{-1} is the PO_2^- symmetric stretch (the dashed red vertical line in Figure 3C,D).[51,53]

The PO_2^- symmetric stretch around 1105 cm^{-1} blue shifted by ∼7 cm^{-1} in the presence of 30 mol % DOTAP (Figure 3C, blue spectrum and dashed blue vertical line, Table S3), indicating that the phosphate moiety dehydrated upon the introduction of the positively charged amphiphile. In addition to the frequency shift, the amplitude of the PO_2^- symmetric stretch was reduced by almost 60%. This change in amplitude can be attributed to a combination of a decrease in the number density of oscillators and a reorientation of the P-N dipole (SI text, Figure S5, Table S3). It should be noted that the attenuation of the PO_2^- resonance occurred concomitantly with an attenuation of the 3200 cm^{-1} peak. On the other hand, the addition of 30 mol % DOPG to the DOPC monolayer led to a small red shift in the PO_2^- symmetric stretch frequency (∼3 cm^{-1}), which indicated enhanced hydration of the DOPG headgroup (Figure 3D, blue spectrum and dashed blue vertical line, Table S4). This supports the proposal that the phosphate−water hydrogen bonding network for DOPC was unperturbed or even perhaps slightly enhanced by the introduction of DOPG. Data at other DOTAP and DOPG concentrations are provided in Figures S6 and S7, respectively.

Deconvolving Changes in Interfacial Water Structure into $\chi^{(2)}$ and $\chi^{(3)}$ Contributions. The 3200 cm^{-1} amplitude from neat DOPC can be nominally attributed to a pure $\chi^{(2)}$ contribution. In the mixed lipid systems studied herein, there is a continuous build-up of surface charge with increasing concentrations of either DOTAP or DOPG in the monolayer. This leads to an increase in the $\chi^{(3)}$ contribution according to eq 2. Moreover, if the $\chi^{(2)}$ term in eq 2 is constant, the 3200 cm^{-1} amplitude should vary linearly with respect to the surface potential. However, the model shown in Figure 1B suggests that the contribution from $\chi^{(2)}$ should not be assumed constant.

Positively charged species, such as DOTAP, while increasing the surface potential, also disrupt the hydrogen bonding network of the water molecules that are directly bonded at the

DOI: 10.1021/acs.jpcb.8b08476
J. Phys. Chem. B 2018, 122, 12260−12270

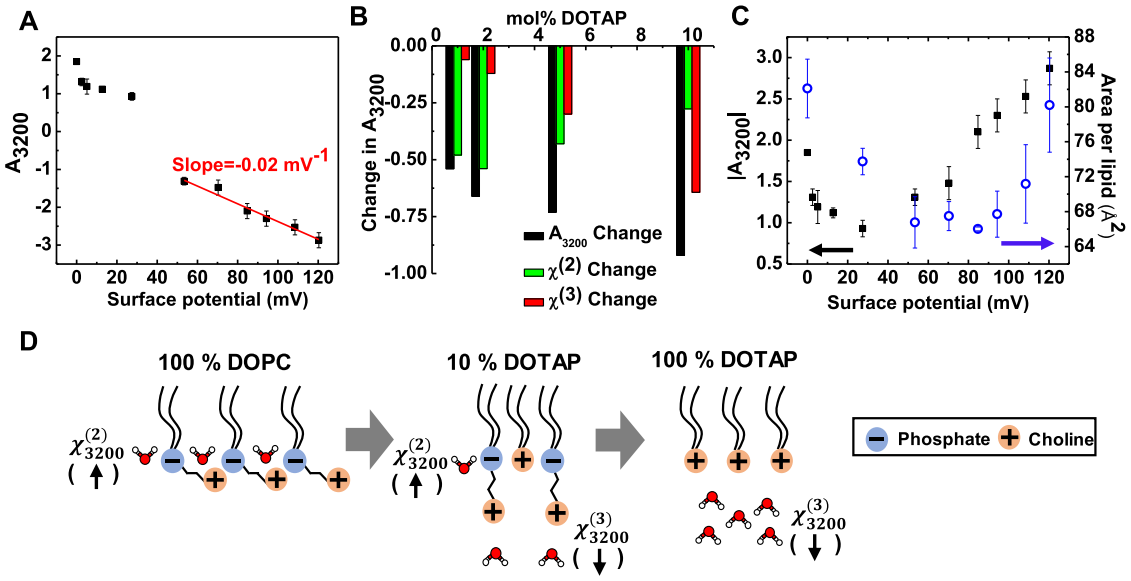

Figure 4. (A) 3200 cm^{-1} amplitudes (A_{3200}) as a function of surface potential. The red line corresponds to a straight line fit for the values above 52 mV. It should be noted that the absolute values of 3200 cm^{-1} amplitude are plotted in Figure 2C to facilitate a direct comparison to the area per lipid measurements. Here, however, both the sign and magnitude of amplitude need to be considered. (B) Change in the amplitude (black) compared to pure DOPC. This value is deconvolved into changes due to $\chi^{(2)}$ (green) and $\chi^{(3)}$ (red). (C) Absolute values of the amplitude (black squares) and area per lipid at 17 mN/m (blue open circles) as a function of surface potential. (D) Schematic diagram illustrating the origin of the 3200 cm^{-1} peak next to DOPC and DOTAP. The black arrows in parentheses below the designation for each type of water represent the signs of the respective contributions.

interface. This should result in an attenuated $\chi^{(2)}$ response. Therefore, the nonmonotonic trends in the OH amplitude as a function of mol % DOTAP should be attributed to both $\chi^{(2)}$ and $\chi^{(3)}$ effects. This idea will be put on a quantitative basis in the discussion below. The relative contributions of $\chi^{(2)}$ and $\chi^{(3)}$ to the overall change in 3200 cm^{-1} amplitude can be estimated by invoking eq 2. To do this, the surface potentials of the mixed DOPC/DOTAP monolayers need to be calculated. This can be done by plugging the surface charge density values obtained from the area per lipid measurements into the Grahame equation (Figure S8).[54] It should be noted here that the surface potential of pure DOPC was assumed to be zero in these calculations. Using these values, the 3200 cm^{-1} amplitudes were plotted against the surface potential values (Figure 4A). As can be seen, the correlation leads to a linear slope from 52 to 120 mV (20 to 100 mol % DOTAP, red line through the data points). This suggests that changes in $\chi^{(3)}$ dominate at higher DOTAP concentrations. As can be seen, the changes in 3200 cm^{-1} amplitude below 52 mV (20 mol % DOTAP) do not fall on this line. Nevertheless, the slope of the straight line can be employed as a scaling factor for the $\chi^{(3)}$ contribution to the 3200 cm^{-1} amplitude and is assumed to be constant at all surface charge densities.[41] The $\chi^{(3)}$ contribution between 1 and 10 mol % DOTAP was therefore calculated to be the product of the slope multiplied by the corresponding surface potential value at each concentration (Figure 4B, red bars). The overall change in the amplitude at each DOTAP concentration compared to pure DOPC is plotted with the black bars in Figure 4B. By invoking eq 2, the change in $\chi^{(2)}$ was then determined as the difference between the overall change in amplitude and the $\chi^{(3)}$ contribution (Figure 4B, green bars).

As can be seen in Figure 4B, the decrease in the OH amplitude between 1 and 10 mol % DOTAP is dominated by $\chi^{(2)}$ changes at the lowest concentration values, but crosses over to a dominant $\chi^{(3)}$ effect as the amount of positive charge is increased. The decrease in amplitude due to changes in $\chi^{(2)}$ is consistent with the loss of directly bonded water molecules from the phosphate groups, which in turn is driven by the decrease in the average area per lipid. The area per lipid continued to decrease up to ~52 mV (20 mol % DOTAP), whereas the magnitude of the OH amplitude at 3200 cm^{-1} decreased only up to ~27 mV (10 mol % DOTAP) (Figure 4C). In fact, the continued decrease in the average area per molecule until 20 mol % DOTAP suggests that $\chi^{(2)}$ should fall until that point. The increasing $\chi^{(3)}$ contribution compensated for this, and the two contributions were of equal magnitude just below 27 mV (~10 mol % DOTAP).

It should be noted that the 3200 cm^{-1} peaks from DOTAP and DOPC have different origins (Figure 4D). Next to DOPC, water molecules directly hydrogen bonded to the phosphate give rise to a 3200 cm^{-1} peak. On the other hand, DOTAP, being a positively charged monolayer, orders water molecules in the subsequent layers that result in a 3200 cm^{-1} peak.[55] Hence, with increasing concentrations of DOTAP, the 3200 cm^{-1} peak switched from water molecules hydrogen bonded to phosphate to water ordered in subsequent layers. As depicted in Figure 4D, these two types of waters should have opposite orientations. As such, the 3200 cm^{-1} peak in DOPC arises from a $\chi^{(2)}$ contribution with a positive sign, whereas the electrostatically ordered water that gives rise to the 3200 cm^{-1} peak from DOTAP has a negative sign and arises from a $\chi^{(3)}$ effect (up arrows depict a positive sign and down arrows depict a negative sign). The minimum in the VSFS signal with 10 mol % DOTAP (~27 mV) (Figure 4C) occurred where the cancelation of these two contributions was most complete. By 20 mol % DOTAP (~52 mV), the majority of the water dipoles giving rise to the 3200 cm^{-1} peak had the opposite orientation, and the increase in the $\chi^{(3)}$ contribution dominated changes in the VSFS signal thereafter.

DOI: 10.1021/acs.jpcb.8b08476
J. Phys. Chem. B 2018, 122, 12260−12270

Next, consider the OH peak around 3600 cm^{-1}, attributed to weakly hydrogen bonded water molecules located in the carbonyl region of the lipid headgroups (Figure 5A, left). The

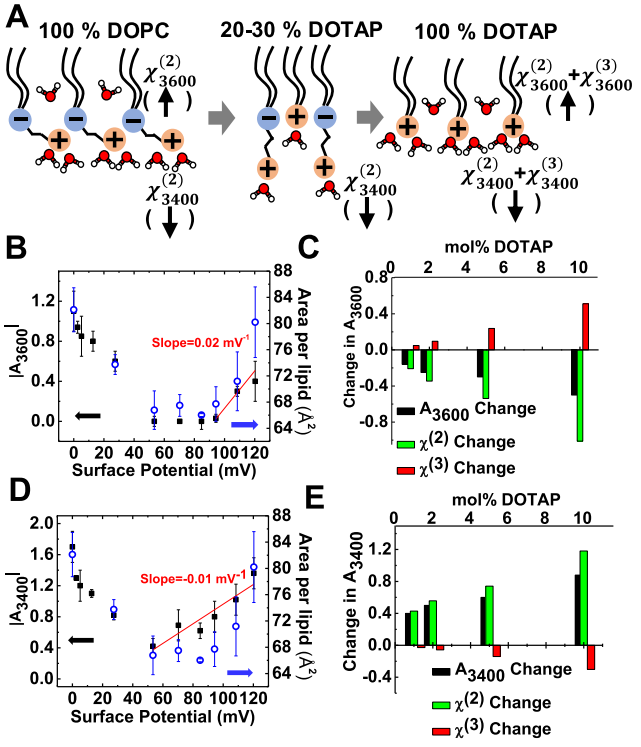

Figure 5. (A) Schematic diagram showing the different water molecules giving rise to the $\chi^{(2)}$ and $\chi^{(3)}$ contributions at 3400 and 3600 cm^{-1}. The black arrows in parenthesis below each water designation represent the sign of the respective contributions. (B) Absolute value of the 3600 cm^{-1} amplitude (black) and area per lipid at 17 mN/m (blue) as a function of the surface potential. The red line corresponds to a linear fit of the values above 93 mV (50 mol % DOTAP). (C) Change in the 3600 cm^{-1} amplitude (black). This change is deconvolved into $\chi^{(2)}$ (green) and $\chi^{(3)}$ (red) contributions. (D) The absolute value of the 3400 cm^{-1} amplitude (black) and the area per lipid at 17 mN/m (blue) as a function of surface potential. The red line corresponds to a linear fit to the data above 52 mV (20 mol % DOTAP). It should be noted that the slope of the linear fit is negative because of the negative sign of the amplitude. (E) Change in the 3400 cm^{-1} amplitude (black). This change is deconvolved into $\chi^{(2)}$ (green) and a $\chi^{(3)}$ (red) contributions.

signal from these water molecules can be assigned to a weak $\chi^{(2)}$ contribution, with a positive sign. This peak has been shown to be sensitive to the surface potential.[56] As can be seen, the magnitude of the amplitude for this peak decreased initially as DOTAP was added to the membrane (Figure 5B, black points). This decrease occurred in tandem with the decrease in area per lipid (Figure 5B, blue points), indicating that these weakly hydrogen bonded water molecules are almost completely squeezed out as the monolayer condensed with the reorientation of the P-N dipole (Figure 5A, center). Above 92 mV (50 mol % DOTAP), however, the 3600 cm^{-1} amplitude picked up again and linearly increased with surface potential after that (Figure 5B, red line). It should be noted that the $\chi^{(3)}$ construct is typically employed to separate the bulk water contribution from the surface contribution. However, the weakly hydrogen bonded water molecules above the DOTAP headgroups contributing to the 3600 cm^{-1} peak are oriented by the electric field (Figure 5A, right). As a result, this peak should have a mixture of $\chi^{(2)}$ and $\chi^{(3)}$ contributions. An analysis similar to that for the 3200 cm^{-1} peak was performed on the 3600 cm^{-1} peak to obtain the relative contributions of each (Figure 5C). This analysis revealed that changes in $\chi^{(2)}$ clearly dominated at low DOTAP concentrations, consistent with the close correlation between the area per lipid and amplitude (Figure 5B). Nevertheless, the $\chi^{(3)}$ contribution continuously grew in, as the concentration of DOTAP was increased.

The 3400 cm^{-1} peak next to both DOPC and DOTAP arose from water molecules with broken hydrogen bonding that were directly adjacent to the quaternary ammonium moiety on the headgroup (Figure 5A). As the DOTAP concentration was increased, the orientation of these water molecules remained constant. As such, the negative sign from the 3400 cm^{-1} peak should be preserved. The magnitude of the 3400 cm^{-1} amplitudes closely followed the decrease in area per molecule and continued to shrink until 52 mV (20 mol % DOTAP) (Figure 5D).

The 3400 cm^{-1} amplitudes above 52 mV could be fit to a straight line to obtain the relative $\chi^{(2)}$ and $\chi^{(3)}$ contributions to the signal change between 2.5 and 27 mV (1−10 mol % DOTAP) (Figure 5E). As can be seen, the changes in the amplitude had a dominant $\chi^{(2)}$ contribution. This should not be surprising due to the proximity of these water molecules to the headgroup.

On the basis of the analysis above, the nonmonotonic trend in the OH stretch region for DOPC/DOTAP monolayers originates from a combination of $\chi^{(2)}$ and $\chi^{(3)}$ effects. These come from changes in the area per lipid and the introduction of charge to the interface. The PC and TAP headgroups differ primarily by the absence of a phosphate group in the latter structure. As the concentration of DOTAP increases, the number of phosphate groups is diminished, whereas the choline part essentially remains the same. This helps to simplify the interpretation of the water spectra.

By contrast, as DOPG is introduced to DOPC, the phosphate groups remain the same, but the choline groups are replaced by glycerol moieties. This makes interpreting the changes a bit more complex. Nevertheless, the VSFS water spectra from DOPC/DOPG monolayers can still largely be understood by using the same analysis as invoked for DOTAP. In this case, both DOPC and DOPG have contributions to the 3200 cm^{-1} peak from water directly hydrogen bonded to the phosphate (Figure 6A, left and right). DOPG, of course, also has a contribution from water aligned by the electric field (Figure 6A, right). The former type of water has a predominant $\chi^{(2)}$ contribution, whereas the latter type arises from a $\chi^{(3)}$ contribution. Unlike DOTAP, DOPG retains the average area per lipid in the lipid monolayer as well as the phosphate hydration. Moreover, all of the water molecules contributing to the 3200 cm^{-1} peak in DOPC/DOPG monolayers have the same orientation. Hence, at low mol % DOPG, the $\chi^{(2)}$ contribution is expected to remain approximately constant and the amplitude should increase linearly, according to eq 2 as DOPG is introduced. This is shown in Figure 6B by plotting the 3200 cm^{-1} amplitudes as a function of surface potential. It should be noted that the x-axis begins at a negative value, as the surface potential is negative at 100% DOPG and rises to zero for pure DOPC. As can be seen, the amplitude between 0 mV and −25 mV (0−10 mol % DOPG) could be fit to a straight line with a constant $\chi^{(2)}$

DOI: 10.1021/acs.jpcb.8b08476
J. Phys. Chem. B 2018, 122, 12260−12270

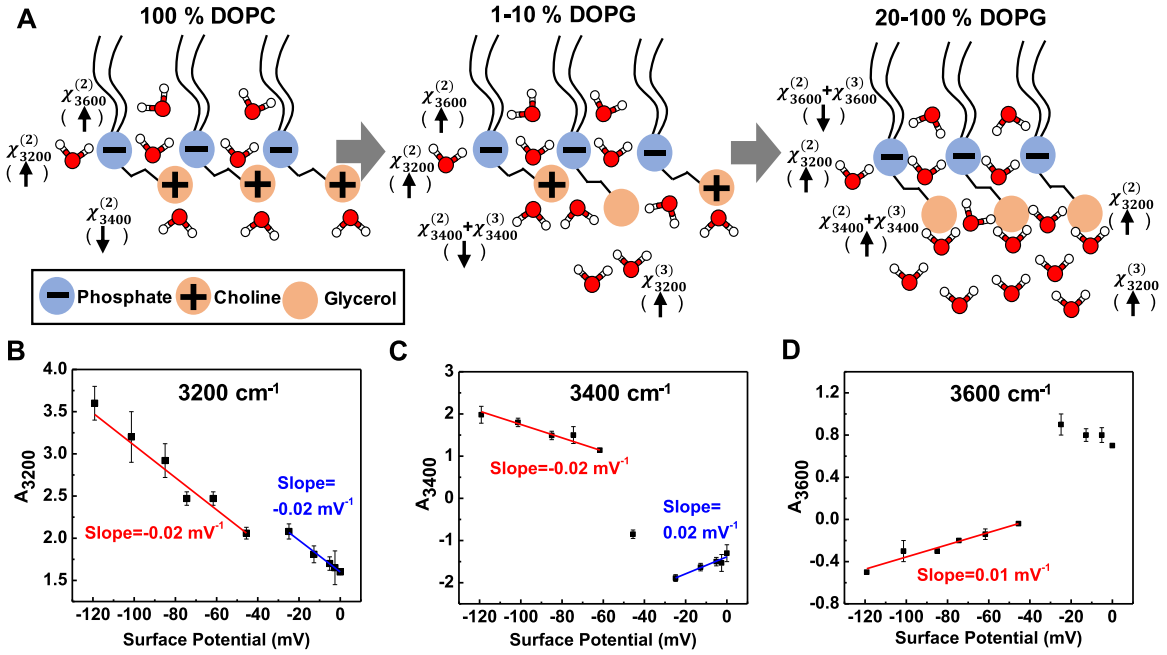

Figure 6. (A) Schematic diagram illustrating the different water molecules giving rise to the $\chi^{(2)}$ and $\chi^{(3)}$ contributions. The black arrows in parenthesis below each water designation represent the sign of the respective contributions. (B) The 3200 cm^{-1} amplitude as a function of the surface potential. The blue line corresponds to a linear fit of data points between 0 and −25 mV (0−10 mol % DOPG) and the red line corresponds to a linear fit of the data points between −45 and −119 mV (20−100 mol % DOPG). (C) The 3400 cm^{-1} amplitude as a function of surface potential. The blue line corresponds to a linear fit of data points between 0 and −25 mV (0−10 mol % DOPG) and the red line corresponds to the a fit between −61 and −119 mV (30−100 mol % DOPG). In this case, the water dipoles flip their net orientation between −25 and −61 mV (10−30 mol % DOPG). (D) The 3600 cm^{-1} amplitude as a function of surface potential. The red line corresponds to a linear fit of the data points between −45 and −119 mV (20−100 mol % DOPG).

contribution close to that of pure DOPC (Figure 6B, blue line).

As with DOPC/DOTAP monolayers, the $\chi^{(3)}$ scaling factor should stay constant for all DOPG concentrations. However, a different constant $\chi^{(2)}$ contribution was required to fit the amplitude of the 3200 cm^{-1} peak above 20 mol % DOPG (−45 mV) (Figure 6B, red line). Indeed, the pure $\chi^{(2)}$ contribution from DOPG should be different from that of DOPC, since the glycerol moiety on DOPG can directly hydrogen bond to water molecules (Figure 6A, right). Presumably, the predominant $\chi^{(2)}$ contribution to the 3200 cm^{-1} signal changes from the $\chi^{(2)}$ of DOPC to the $\chi^{(2)}$ of DOPG. As a result of the unchanged area per lipid, the amplitudes of the 3400 and 3600 cm^{-1} peaks also exhibited linear trends, similar to the 3200 cm^{-1} peak (Figure 6C,D). The different origins of the 3400 cm^{-1} peak around DOPC and DOPG are illustrated in Figure 6A. Between 0 and 10 mol % DOPG (0 to −25 mV), the amplitude from the 3400 cm^{-1} peak retains the negative sign and increases in magnitude with added DOPG (Figure 6C, blue line). This increase can be attributed to increased hydration around the choline group, facilitated by the neighboring glycerol moiety from DOPG. However, the 3400 cm^{-1} peak next to DOPG arises from water molecules around the glycerol moiety.[55] These water molecules have opposite orientation to those around choline. As such, a flip in the sign of the 3400 cm^{-1} oscillator is observed between 10 and 30 mol % DOPG (−25 to −61 mV). Above 30 mol % DOPG (−61 mV), a linear trend was again observed (Figure 6C, red line). Finally, the 3600 cm^{-1} amplitude remained approximately constant below 10 mol % DOPG (−25 mV) (Figure 6D). By 20 mol % DOPG (−45 mV), however, the surface potential on the monolayer built up sufficiently to flip the orientation of these water molecules (Figure 6A, right), and the changes in amplitude thereafter could be fit to a straight line (Figure 6D, red line).

It is evident from the data in Figures 4−6 that the $\chi^{(3)}$ contribution to the VSFS signal varies linearly with respect to the surface potential. This agrees with the prediction of eq 2. It should be noted, however, that this simplified form of the $\chi^{(3)}$ contribution in eq 2 is valid because the subphase solutions in these experiments were held at a constant ionic strength of 110 mM as the mole fraction of charged lipids was increased. This corresponds to a Debye length of just ∼0.9 nm, which is equivalent to approximately three layers of water. Therefore, the experiments herein are probing the $\chi^{(2)}$ and $\chi^{(3)}$ contributions from just the first few layers of water, which includes a very substantial contribution from water molecules that are directly hydrogen bonded to the headgroup. For solutions with lower ionic strengths, increasing the surface potential will align more water molecules further away from the surface. This would lead to a larger probing depth that would, in turn, modify the $\chi^{(3)}$ contribution into a complex term that depends on the Debye length.[39,57,58] In fact, the low concentration dip in the fitted amplitude data from DOPC/DOTAP monolayers in Figure 2C can be greatly attenuated when otherwise identical experiments are performed on a subphase with an ionic strength of only 10 mM (Figure S9). The attenuated dip in that case is a direct result of the greater probing depth and interference.

Interfacial Water Structure Next to the P-N Dipole Can Be Modulated by a Wide Range of Positive and Negative Charges in a General Fashion. In a final set of VSFS measurements, we tested the effects of positively and negatively charged ions and small molecules on the interfacial

DOI: 10.1021/acs.jpcb.8b08476
J. Phys. Chem. B 2018, 122, 12260−12270

water structure adjacent to DOPC monolayers. Ca^{2+} and SCN^- have previously been shown to bind to PC lipids in membranes.[59−61] To test if these ions have opposite effects on interfacial water structure, we recorded the VSFS spectra of DOPC monolayers in the presence of 1 M $CaCl_2$ (Figure 7A)

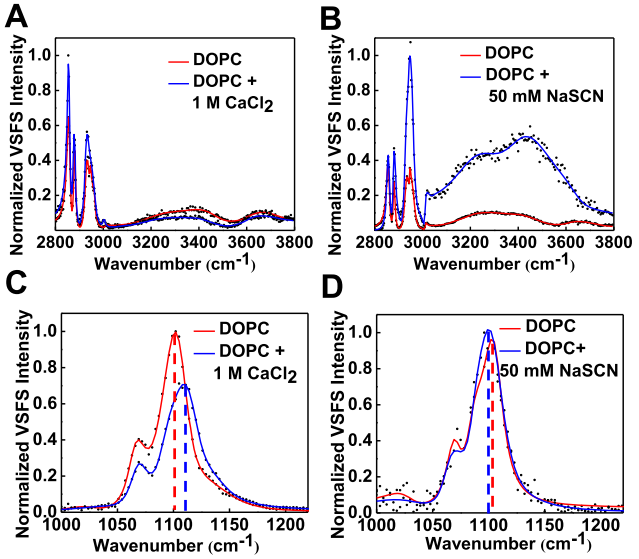

Figure 7. Effects of cations and anions on the interfacial water structure next to DOPC. VSFS spectra of the CH and OH stretch regions from DOPC monolayers (A) in the absence and presence of 1 M $CaCl_2$ as well as (B) in the absence and presence of 50 mM NaSCN. The PO_2^- symmetric stretch of DOPC (C) with and without 1 M $CaCl_2$ as well as (D) in the presence and absence of 50 mM NaSCN. The ionic strength was held constant for each experiment by using the appropriate concentration of NaCl as the background. Specifically, the spectra with $CaCl_2$ were compared to a subphase containing 3 M NaCl and 10 mM Tris. The spectra with NaSCN were performed with 50 mM NaSCN and 50 mM NaCl in the subphase and were compared against a buffer solution containing 100 mM NaCl and 10 mM Tris. MEM analysis of these spectra is provided in Figure S11, and the fitted results are tabulated in Tables S5−S7.

and 50 mM NaSCN (Figure 7B) in the subphase. Each spectrum was compared to a reference spectrum of DOPC measured on a buffer subphase containing the same ionic strength, but replaced with NaCl. The Na^+ and Cl^- counterions in these experiments do not significantly interact with the monolayers (Figure S10). As such, the changes with Ca^{2+} and SCN^- can be attributed almost exclusively to these two ions themselves, rather than their counterions.

Compared to a subphase with 3 M NaCl, 1 M Ca^{2+} moderately attenuated the intensity of the 3200 cm^{-1} peak. By contrast, 50 mM SCN^- enhanced the water peaks quite substantially. The binding of SCN^- to the lipid monolayer made it negatively charged[62] and this led to an enhanced ordering of water molecules. The binding of Ca^{2+} was much weaker,[59,63] but nevertheless led to a net positive charge at the interface. These changes in interfacial water structure are analogous to the changes found by embedding charged lipids. Also, in the PO_2^-symmetric stretch region, Ca^{2+} induced a blue shift in the frequency of the PO_2^- symmetric stretch (Figure 7C), in agreement with previous studies.[49] Moreover, SCN^- resulted in a slight red shift (~1 cm^{-1}) of the PO_2^- symmetric stretch frequency (Figure 7D), indicating that the hydrogen bonding environment of phosphate was still preserved or slightly strengthened. To test if the trends in the area per molecule observed for positively and negatively charged lipids were also valid for ions, we measured the surface pressure−area isotherms of DOPC in the presence of Ca^{2+} and SCN^- ions. In fact, Ca^{2+} caused the monolayer to contract, whereas SCN^- expanded it (Figure S12). The increase in area per lipid molecule with SCN^- was not entirely unexpected, since SCN^- can insert itself into liquid expanded monolayer phases.[64]

We further tested the generality of the correlation between the interfacial water spectrum and the hydrogen bonding environment around phosphate by using positively and negatively charged small molecules. For this purpose, tetracaine and ibuprofen were employed, which are two common small molecule drugs that are known to bind to PC lipid.[66,67] The counterions were Cl^- and Na^+. Tetracaine has a protonated dimethylamino moiety, making it positively charged near neutral pH (Figure 8A). The carboxylate moiety

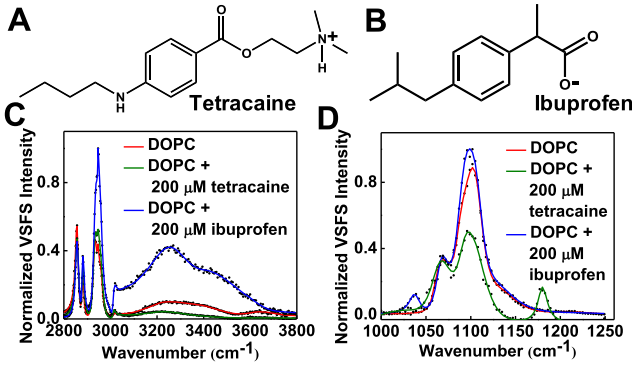

Figure 8. Structures of (A) tetracaine and (B) ibuprofen. (C) VSFS spectra of interfacial water next to DOPC in the presence of 200 μM tetracaine (green) and 200 μM ibuprofen (blue). (D) PO_2^- symmetric stretch spectra of DOPC with 200 μM tetracaine (green) and 200 μM ibuprofen (blue) in the subphase as well as the spectrum without these molecules (red). All spectra were recorded on buffer solutions containing 10 mM Tris and 100 mM NaCl at pH 7.4. MEM analysis of the spectra is provided in Figure S14, and the fitted results are tabulated in Tables S8−S10. It should be noted that the small feature at 1180 cm^{-1} in the presence of tetracaine arises from the tetracaine molecule itself.[65]

on ibuprofen is deprotonated at physiological pH, leading to an overall negative charge (Figure 8B). VSFS spectra of DOPC monolayers were recorded with 200 μM tetracaine or ibuprofen in the subphase (Figure 8C). As can be seen, tetracaine decreased the intensity of the 3200 cm^{-1} peak (green), whereas ibuprofen increased it (blue). Interestingly, neither of these molecules blue shifted the frequency of the phosphate symmetric stretch (Figure 8D). The observation that ibuprofen does not cause a blue shift agrees well with our prediction based on its negative charge. Additionally, ibuprofen was found to increase the average area per headgroup in the DOPC monolayer (Figure S13).

The lack of a blue shift by tetracaine is intriguing. Tetracaine's exceptional behavior can probably be attributed to its mode of interaction. Previous studies on the interactions of tetracaine with PC lipids have shown that charge is not the only factor that influences its binding.[68] Tetracaine inserts itself into lipid membranes, and the butylamino group resides in the hydrophobic tail region. The protonated dimethylamino moiety is located right next to the phosphate of the PC headgroup. As such, the dimethylamino moiety should directly

DOI: 10.1021/acs.jpcb.8b08476
J. Phys. Chem. B 2018, 122, 12260−12270

hydrogen bond with the phosphate. This hydrogen bonding is apparently quite similar to water−phosphate hydrogen bonding and does not cause a blue shift in the vibrational frequency of the phosphate symmetric stretch. We further measured the surface pressure−area isotherm of DOPC in the presence of 200 μM tetracaine in the subphase (Figure S13). Unlike DOTAP and Ca^{2+}, the average area per molecule was found to increase in the presence of tetracaine. This can be attributed to the difference in the mechanism of interaction of tetracaine with PC. In addition to electrostatic and hydrogen bonding interactions, tetracaine molecules insert themselves into the monolayer through hydrophobic interactions, causing an increase in the total area of the monolayer. This change occurs because of the additional hydrophobic moiety rather than an increase in the average area per lipid (See SI *text* for an additional note on area per lipid measurements).

Remarkably, the introduction of ions and small molecules gave rise to similar changes in interfacial water to those found with charged lipids. The general trends observed here for positive and negative charges (with the partial exception of tetracaine) should be useful in predicting the changes in hydration next to zwitterionic lipid membrane interfaces in the presence of a wide variety of chemistries (e.g., charged amphiphiles, drug molecules, ions, and even peptides). Moreover, the model developed here for $\chi^{(3)}$ changes in the VSFS spectra strongly suggests that changes in the amplitude in the OH stretch region due to the $\chi^{(3)}$ contribution simply vary linearly with interfacial potential. This model should be useful for interpreting other nonlinear optical experiments at aqueous interfaces.

■ ASSOCIATED CONTENT

Supporting Information

The Supporting Information is available free of charge on the ACS Publications website at DOI: 10.1021/acs.jpcb.8b08476.

Material and methods; detailed description of VSFS spectral fitting; notes on estimating surface potential and calculation of area per molecule; complete set of VSFS spectra of DOPC with increasing concentrations of DOTAP and DOPG; imaginary $\chi^{(2)}$ spectra from MEM; full set of pressure−area isotherms of DOPC with increasing concentrations of DOTAP and DOPG; phosphate spectra of 30 mol % DOTAP under different polarization combinations; phosphate spectra of DOPC with varying mol % DOTAP; comparison of phosphate spectra of DOPC and DOPG; calculated surface potentials from Grahame equation plotted as a function of mol % DOTAP; effect of decrease in ionic strength on the absolute value of 3200 cm^{-1} amplitude; OH stretch region of DOPC with 100 mM and 3 M NaCl; pressure−area isotherms of DOPC with positively and negatively charged ions and small molecules; fluorescence image of a DOPC monolayer; tables with VSFS fitting parameters (PDF)

■ AUTHOR INFORMATION

Corresponding Author

*E-mail: psc11@psu.edu.

ORCID

Saranya Pullanchery: 0000-0002-7011-0788

Paul S. Cremer: 0000-0002-8524-0438

Notes

The authors declare no competing financial interest.

■ ACKNOWLEDGMENTS

We acknowledge the National Science Foundation (CHE-1709735) for funding this project. We thank Bradley A. Rogers for critical feedback on the manuscript.

■ REFERENCES

(1) Du, Q.; Superfine, R.; Freysz, E.; Shen, Y. R. Vibrational spectroscopy of water at the vapor/water interface. *Phys. Rev. Lett.* **1993**, *70*, 2313−2316.

(2) Richmond, G. L. Molecular Bonding and Interactions at Aqueous Surfaces as Probed by Vibrational Sum Frequency Spectroscopy. *Chem. Rev.* **2002**, *102*, 2693−2724.

(3) Shen, Y. R. *The Principles of Nonlinear Optics*; Wiley: New York, 2003.

(4) Lambert, A. G.; Davies, P. B.; Neivandt, D. J. Implementing the Theory of Sum Frequency Generation Vibrational Spectroscopy: A Tutorial Review. *Appl. Spectrosc. Rev.* **2005**, *40*, 103−145.

(5) Shen, Y. R.; Ostroverkhov, V. Sum-Frequency Vibrational Spectroscopy on Water Interfaces: Polar Orientation of Water Molecules at Interfaces. *Chem. Rev.* **2006**, *106*, 1140−1154.

(6) Zhu, X. D.; Suhr, H.; Shen, Y. R. Surface vibrational spectroscopy by infrared-visible sum frequency generation. *Phys. Rev. B* **1987**, *35*, 3047−3050.

(7) Guyot-Sionnest, P.; Hunt, J. H.; Shen, Y. R. Sum-frequency vibrational spectroscopy of a Langmuir film: Study of molecular orientation of a two-dimensional system. *Phys. Rev. Lett.* **1987**, *59*, 1597−1600.

(8) Walker, R. A.; Gruetzmacher, J. A.; Richmond, G. L. Phosphatidylcholine Monolayer Structure at a Liquid−Liquid Interface. *J. Am. Chem. Soc.* **1998**, *120*, 6991−7003.

(9) Kim, J.; Kim, G.; Cremer, P. S. Investigations of Water Structure at the Solid/Liquid Interface in the Presence of Supported Lipid Bilayers by Vibrational Sum Frequency Spectroscopy. *Langmuir* **2001**, *17*, 7255−7260.

(10) Watry, M. R.; Tarbuck, T. L.; Richmond, G. L. Vibrational Sum-Frequency Studies of a Series of Phospholipid Monolayers and the Associated Water Structure at the Vapor/Water Interface. *J. Phys. Chem. B.* **2003**, *107*, 512−518.

(11) Nihonyanagi, S.; Yamaguchi, S.; Tahara, T. Direct evidence for orientational flip-flop of water molecules at charged interfaces: A heterodyne-detected vibrational sum frequency generation study. *J. Chem. Phys.* **2009**, *130*, No. 204704.

(12) Chen, X.; Hua, W.; Huang, Z.; Allen, H. C. Interfacial Water Structure Associated with Phospholipid Membranes Studied by Phase-Sensitive Vibrational Sum Frequency Generation Spectroscopy. *J. Am. Chem. Soc.* **2010**, *132*, 11336−11342.

(13) Lopez, C. F.; Nielsen, S. O.; Klein, M. L.; Moore, P. B. Hydrogen Bonding Structure and Dynamics of Water at the Dimyristoylphosphatidylcholine Lipid Bilayer Surface from a Molecular Dynamics Simulation. *J. Phys. Chem. B* **2004**, *108*, 6603−6610.

(14) Mondal, J. A.; Nihonyanagi, S.; Yamaguchi, S.; Tahara, T. Three Distinct Water Structures at a Zwitterionic Lipid/Water Interface Revealed by Heterodyne-Detected Vibrational Sum Frequency Generation. *J. Am. Chem. Soc.* **2012**, *134*, 7842−7850.

(15) Roy, S.; Gruenbaum, S. M.; Skinner, J. L. Theoretical vibrational sum-frequency generation spectroscopy of water near lipid and surfactant monolayer interfaces. *J. Chem. Phys.* **2014**, *141*, No. 18C502.

(16) Re, S.; Nishima, W.; Tahara, T.; Sugita, Y. Mosaic of Water Orientation Structures at a Neutral Zwitterionic Lipid/Water Interface Revealed by Molecular Dynamics Simulations. *J. Phys. Chem. Lett.* **2014**, *5*, 4343−4348.

(17) Roy, S.; Gruenbaum, S. M.; Skinner, J. L. Theoretical vibrational sum-frequency generation spectroscopy of water near

lipid and surfactant monolayer interfaces. II. Two-dimensional spectra. *J. Chem. Phys.* **2014**, *141*, No. 22D505.
(18) Ishiyama, T.; Terada, D.; Morita, A. Hydrogen-Bonding Structure at Zwitterionic Lipid/Water Interface. *J. Phys. Chem. Lett.* **2016**, *7*, 216−220.
(19) Hua, W.; Verreault, D.; Allen, H. C. Solvation of Calcium−Phosphate Headgroup Complexes at the DPPC/Aqueous Interface. *ChemPhysChem* **2015**, *16*, 3910−3915.
(20) Viswanath, P.; Aroti, A.; Motschmann, H.; Leontidis, E. Vibrational Sum Frequency Generation Spectroscopic Investigation of the Interaction of Thiocyanate Ions with Zwitterionic Phospholipid Monolayers at the Air−Water Interface. *J. Phys. Chem. B* **2009**, *113*, 14816−14823.
(21) Wu, F.-G.; Yang, P.; Zhang, C.; Han, X.; Song, M.; Chen, Z. Investigation of Drug−Model Cell Membrane Interactions Using Sum Frequency Generation Vibrational Spectroscopy: A Case Study of Chlorpromazine. *J. Phys. Chem. C* **2014**, *118*, 17538−17548.
(22) Li, B.; Wang, H.-Y.; Feng, P.; Han, X.; Chen, Z.; Lu, X.; Wu, F.-G. Qualitative and Quantitative Analyses of the Molecular-Level Interaction between Memantine and Model Cell Membranes. *J. Phys. Chem. C* **2015**, *119*, 17074−17083.
(23) Toledo-Fuentes, X.; Lis, D.; Cecchet, F. Structural Changes to Lipid Bilayers and Their Surrounding Water upon Interaction with Functionalized Gold Nanoparticles. *J. Phys. Chem. C* **2016**, *120*, 21399−21409.
(24) Büldt, G.; Gally, H. U.; Seelig, J.; Zaccai, G. Neutron diffraction studies on phosphatidylcholine model membranes. *J. Mol. Biol.* **1979**, *134*, 673−691.
(25) Hauser, H.; Pascher, I.; Pearson, R. H.; Sundell, S. Preferred conformation and molecular packing of phosphatidylethanolamine and phosphatidylcholine. *Biochim. Biophys. Acta, Rev. Biomembr.* **1981**, *650*, 21−51.
(26) Wiener, M. C.; White, S. H. Structure of a fluid dioleoylphosphatidylcholine bilayer determined by joint refinement of x-ray and neutron diffraction data. III. Complete structure. *Biophys. J.* **1992**, *61*, 434−447.
(27) Altenbach, C.; Seelig, J. Calcium binding to phosphatidylcholine bilayers as studied by deuterium magnetic resonance. Evidence for the formation of a calcium complex with two phospholipid molecules. *Biochemistry* **1984**, *23*, 3913−3920.
(28) Macdonald, P. M.; Seelig, J. Anion binding to neutral and positively-charged lipid membranes. *Biochemistry* **1988**, *27*, 6769−6775.
(29) Seelig, A.; Allegrini, P. R.; Seelig, J. Partitioning of local anesthetics into membranes: surface charge effects monitored by the phospholipid head-group. *Biochim. Biophys. Acta, Biomembr.* **1988**, *939*, 267−276.
(30) Scherer, P. G.; Seelig, J. Electric charge effects on phospholipid headgroups. Phosphatidylcholine in mixtures with cationic and anionic amphiphiles. *Biochemistry* **1989**, *28*, 7720−7728.
(31) Kuchinka, E.; Seelig, J. Interaction of melittin with phosphatidylcholine membranes. Binding isotherm and lipid head-group conformation. *Biochemistry* **1989**, *28*, 4216−4221.
(32) Zhao, W.; Gurtovenko, A. A.; Vattulainen, I.; Karttunen, M. Cationic Dimyristoylphosphatidylcholine and Dioleoyloxytrimethylammonium Propane Lipid Bilayers: Atomistic Insight for Structure and Dynamics. *J. Phys. Chem. B* **2012**, *116*, 269−276.
(33) Gurtovenko, A. A.; Patra, M.; Karttunen, M.; Vattulainen, I. Cationic DMPC/DMTAP Lipid Bilayers: Molecular Dynamics Study. *Biophys. J.* **2004**, *86*, 3461−3472.
(34) Shen, Y. R. Surface properties probed by second-harmonic and sum-frequency generation. *Nature* **1989**, *337*, 519−525.
(35) Zhao, X.; Ong, S.; Eisenthal, K. B. Polarization of water molecules at a charged interface. Second harmonic studies of charged monolayers at the air/water interface. *Chem. Phys. Lett.* **1993**, *202*, 513−520.
(36) Eisenthal, K. B. Liquid Interfaces Probed by Second-Harmonic and Sum-Frequency Spectroscopy. *Chem. Rev.* **1996**, *96*, 1343−1360.
(37) de Beer, A. G. F.; Campen, R. K.; Roke, S. Separating surface structure and surface charge with second-harmonic and sum-frequency scattering. *Phys. Rev. B* **2010**, *82*, No. 235431.
(38) Jena, K. C.; Covert, P. A.; Hore, D. K. The Effect of Salt on the Water Structure at a Charged Solid Surface: Differentiating Second- and Third-order Nonlinear Contributions. *J. Phys. Chem. Lett.* **2011**, *2*, 1056−1061.
(39) Ohno, P. E.; Wang, H.-f.; Geiger, F. M. Second-order spectral lineshapes from charged interfaces. *Nat. Commun.* **2017**, *8*, No. 1032.
(40) Rao, Y.; Kwok, S. J. J.; Lombardi, J.; Turro, N. J.; Eisenthal, K. B. Label-free probe of HIV-1 TAT peptide binding to mimetic membranes. *Proc. Natl. Acad. Sci. USA* **2014**, *111*, 12684−12688.
(41) Wen, Y.-C.; Zha, S.; Liu, X.; Yang, S.; Guo, P.; Shi, G.; Fang, H.; Shen, Y. R.; Tian, C. Unveiling Microscopic Structures of Charged Water Interfaces by Surface-Specific Vibrational Spectroscopy. *Phys. Rev. Lett.* **2016**, *116*, No. 016101.
(42) DeWalt-Kerian, E. L.; Kim, S.; Azam, M. S.; Zeng, H.; Liu, Q.; Gibbs, J. M. pH-Dependent Inversion of Hofmeister Trends in the Water Structure of the Electrical Double Layer. *J. Phys. Chem. Lett.* **2017**, *8*, 2855−2861.
(43) Sovago, M.; Vartiainen, E.; Bonn, M. Determining Absolute Molecular Orientation at Interfaces: A Phase Retrieval Approach for Sum Frequency Generation Spectroscopy. *J. Phys. Chem. C* **2009**, *113*, 6100−6106.
(44) de Beer, A. G. F.; Samson, J.-S.; Hua, W.; Huang, Z.; Chen, X.; Allen, H. C.; Roke, S. Direct comparison of phase-sensitive vibrational sum frequency generation with maximum entropy method: Case study of water. *J. Chem. Phys.* **2011**, *135*, No. 224701.
(45) Jena, K. C.; Hore, D. K. Variation of Ionic Strength Reveals the Interfacial Water Structure at a Charged Mineral Surface. *J. Phys. Chem. C* **2009**, *113*, 15364−15372.
(46) Darlington, A. M.; Jarisz, T. A.; DeWalt-Kerian, E. L.; Roy, S.; Kim, S.; Azam, M. S.; Hore, D. K.; Gibbs, J. M. Separating the pH-Dependent Behavior of Water in the Stern and Diffuse Layers with Varying Salt Concentration. *J. Phys. Chem. C* **2017**, *121*, 20229−20241.
(47) Yeganeh, M. S.; Dougal, S. M.; Pink, H. S. Vibrational Spectroscopy of Water at Liquid/Solid Interfaces: Crossing the Isoelectric Point of a Solid Surface. *Phys. Rev. Lett.* **1999**, *83*, 1179−1182.
(48) Kataoka, S.; Gurau, M. C.; Albertorio, F.; Holden, M. A.; Lim, S.-M.; Yang, R. D.; Cremer, P. S. Investigation of Water Structure at the TiO2/Aqueous Interface. *Langmuir* **2004**, *20*, 1662−1666.
(49) Casillas-Ituarte, N. N.; Chen, X.; Castada, H.; Allen, H. C. Na+ and Ca2+ Effect on the Hydration and Orientation of the Phosphate Group of DPPC at Air−Water and Air−Hydrated Silica Interfaces. *J. Phys. Chem. B* **2010**, *114*, 9485−9495.
(50) Smolentsev, N.; Lütgebaucks, C.; Okur, H. I.; de Beer, A. G. F.; Roke, S. Intermolecular Headgroup Interaction and Hydration as Driving Forces for Lipid Transmembrane Asymmetry. *J. Am. Chem. Soc.* **2016**, *138*, 4053−4060.
(51) Casal, H. L.; Mantsch, H. H.; Paltauf, F.; Hauser, H. Infrared and 31P-NMR studies of the effect of Li+ and Ca2+ on phosphatidylserines. *Biochim. Biophys. Acta, Lipids Lipid Metab.* **1987**, *919*, 275−286.
(52) Mrázková, E.; Hobza, P.; Bohl, M.; Gauger, D. R.; Pohle, W. Hydration-Induced Changes of Structure and Vibrational Frequencies of Methylphosphocholine Studied as a Model of Biomembrane Lipids. *J. Phys. Chem. B* **2005**, *109*, 15126−15134.
(53) Liljeblad, J. F. D.; Bulone, V.; Tyrode, E.; Rutland, M. W.; Johnson, C. M. Phospholipid Monolayers Probed by Vibrational Sum Frequency Spectroscopy: Instability of Unsaturated Phospholipids. *Biophys. J.* **2010**, *98*, L50−L52.
(54) Israelachvili, J. N. Electrostatic Forces between Surfaces in Liquids. *Intermolecular and Surface Forces*, 3rd ed.; Academic Press: San Diego, 2011; pp 291−340, Chapter 14.
(55) Gurau, M. C.; Kim, G.; Lim, S.-M.; Albertorio, F.; Fleisher, H. C.; Cremer, P. S. Organization of Water Layers at Hydrophilic Interfaces. *ChemPhysChem* **2003**, *4*, 1231−1233.

DOI: 10.1021/acs.jpcb.8b08476
J. Phys. Chem. B 2018, 122, 12260−12270

(56) Nojima, Y.; Suzuki, Y.; Yamaguchi, S. Weakly Hydrogen-Bonded Water Inside Charged Lipid Monolayer Observed with Heterodyne-Detected Vibrational Sum Frequency Generation Spectroscopy. *J. Phys. Chem. C* **2017**, *121*, 2173−2180.
(57) Gonella, G.; Lütgebaucks, C.; de Beer, A. G. F.; Roke, S. Second Harmonic and Sum-Frequency Generation from Aqueous Interfaces Is Modulated by Interference. *J. Phys. Chem. C* **2016**, *120*, 9165−9173.
(58) Ohno, P. E.; Saslow, S. A.; Wang, H.-f.; Geiger, F. M.; Eisenthal, K. B. Phase-referenced nonlinear spectroscopy of the α-quartz/water interface. *Nat. Commun.* **2016**, *7*, No. 13587.
(59) McLaughlin, A.; Grathwohl, C.; McLaughlin, S. The adsorption of divalent cations to phosphatidylcholine bilayer membranes. *Biochim. Biophys. Acta, Biomembr.* **1978**, *513*, 338−357.
(60) Cunningham, B. A.; Lis, L. J. Thiocyanate and bromide ions influence the bilayer structural parameters of phosphatidylcholine bilayers. *Biochim. Biophys. Acta, Biomembr.* **1986**, *861*, 237−242.
(61) Aroti, A.; Leontidis, E.; Dubois, M.; Zemb, T. Effects of Monovalent Anions of the Hofmeister Series on DPPC Lipid Bilayers Part I: Swelling and In-Plane Equations of State. *Biophys. J.* **2007**, *93*, 1580−1590.
(62) McLaughlin, S.; Bruder, A.; Chen, S.; Moser, C. Chaotropic anions and the surface potential of bilayer membranes. *Biochim. Biophys. Acta, Biomembr.* **1975**, *394*, 304−313.
(63) Poyton, M. F.; Sendecki, A. M.; Cong, X.; Cremer, P. S. Cu2+ Binds to Phosphatidylethanolamine and Increases Oxidation in Lipid Membranes. *J. Am. Chem. Soc.* **2016**, *138*, 1584−1590.
(64) Aroti, A.; Leontidis, E.; Maltseva, E.; Brezesinski, G. Effects of Hofmeister Anions on DPPC Langmuir Monolayers at the Air−Water Interface. *J. Phys. Chem. B* **2004**, *108*, 15238−15245.
(65) Shibata, A.; Ikawa, K.; Terada, H. Site of action of the local anesthetic tetracaine in a phosphatidylcholine bilayer with incorporated cardiolipin. *Biophys. J.* **1995**, *69*, 470−477.
(66) Fox, C. B.; Horton, R. A.; Harris, J. M. Detection of Drug−Membrane Interactions in Individual Phospholipid Vesicles by Confocal Raman Microscopy. *Anal. Chem.* **2006**, *78*, 4918−4924.
(67) Huang, D.; Zhao, T.; Xu, W.; Yang, T.; Cremer, P. S. Sensing Small Molecule Interactions with Lipid Membranes by Local pH Modulation. *Anal. Chem.* **2013**, *85*, 10240−10248.
(68) Hutterer, R.; Krämer, K.; Schneider, F. W.; Hof, M. The localization of the local anesthetic tetracaine in phospholipid vesicles: A fluorescence quenching and resonance energy transfer study. *Chem. Phys. Lipids* **1997**, *90*, 11−23.

DOI: 10.1021/acs.jpcb.8b08476
J. Phys. Chem. B 2018, 122, 12260−12270